
High Quality Bi-Linear Transfinite Meshing with Interior Point Constraints

Nilanjan Mukherjee

Meshing & Abstraction Group, Digital Simulation Solutions UGS
2000 Eastman Dr, Milford, OH 45150, USA
nilanjan.mukherjee@ugs.com

Abstract. For a variety of structural finite element analyses on automotive body panels, aerospace wings and space satellite panels, high-quality, structured quadrilateral meshing is imperative. Transfinite meshing, the technique to produce such meshes is severely infringed by the presence of surface-interior point constraints. The present paper attempts to solve the inverse problem of transfinite meshing with interior point constraints. A modified Newton Raphson based solution is proposed to inverse solve Coons bi-linear blending equation. The Coons parametric coordinates are thus determined for a set of face-interior points from their global coordinates. The boundary of the surface is next seeded with “soft-points” at reflected locations and smart-discretized to result in high fidelity, high-quality transfinite meshes.

Keywords: Point constraint, mesh, transfinite, mapped, structured, Coon's Equation, Newton-Raphson

1. Introduction

Mapped meshing or transfinite meshing is an important mesh generation technique, especially with quads, used frequently in a wide gamut of finite element analysis problems. These meshes are structured and hence have a higher solution reliability. These meshes are also economical and if stress-sensitive regions of the outer surface are pre-meshed with such meshes, a lighter tetrahedral mesh is usually produced. However, interior mesh points are hard to honor for transfinite meshes. Usually the nearest node is snapped to the interior point. This depletes element quality often. In the

present paper, an attempt is made to solve the inverse problem of transfinite meshing with interior point constraints. The inverse problem is solved to evaluate Coons parametric coordinates of the interior point constraints from their global world coordinates. A conventional modified Newton-Raphson based solution is proposed to inverse solve Coons' bilinear blending equation. The boundary of the surface is next seeded with "soft-points" at reflected locations and smart-discretized.

2. Past Research

Mapped or transfinite meshing techniques with both quadrilateral and triangular elements remain to be one of the earliest automatic mesh generation algorithms in the world of surface mesh generation. Zienkiewicz and Phillips [1] report probably one of the earliest papers in this area. They proposed a 2D automatic mesh generation scheme based on isoparametric mapping for flat and curved surfaces. Gordon and Hall [2] defined the transfinite interpolation on the rectangle two years later in 1973. In 1974, Cook [3] used it to construct C^0 continuous quadrangulations of deformed quadrangles. Cook's method induces C^0 continuous structured meshes on C^0 continuous transfinite patches. Haber et al. [4] discuss a general purpose transfinite mapping technique for a wide range of surfaces. Alain Peronnet [5–7] did several in-depth investigations on transfinite interpolation techniques on both C^1 and G^1 continuous domains for both 2D and 3D surfaces. Mitchell [8–9] and Armstrong [10] reported approaches to automatically identify the corners of a mapped meshable domain and discuss techniques to assign intervals on surface boundaries. However, even after an exhaustive research, no research work was found on the transfinite mesh generation problem with interior point constraints.

3. Problem Statement

The present paper attempts to solve the problem of generating a transfinite mesh on a face geometry such that the grid lines pass through a set of face interior point constraints. When that is attained, a nice smooth structured mesh is produced that has high quality surface elements that are not distracted by the interior constraints. Fig. 1 shows a regular mapped mesh where the interior point constraints are ignored.

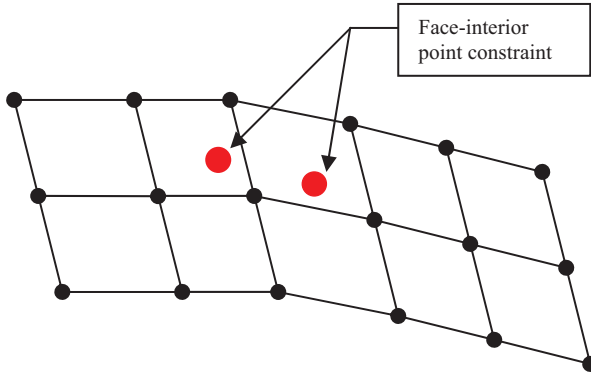


Fig. 1. A mapped mesh with interior constraints ignored

Figure 2 depicts the same geometry with the same mesh, where the interior mesh nodes are snapped to the constraints that are nearest to them. No mesh node is allowed to snap to more than one point constraint, else the topology of the mesh will collapse at that location. The boundary discretization remains unchanged.

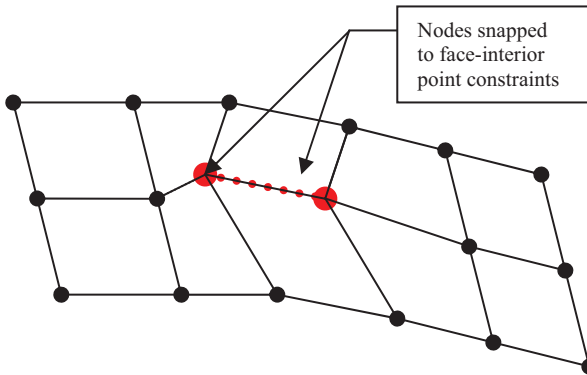


Fig. 2. Mapped mesh with mesh nodes snapped to the nearest interior constraints

When nearest nodes are snapped to the interior mesh points, the element shapes distort resulting in highly skewed elements that are unreliable for stress and dynamic structural analysis. Automobile car body panels need to model arrays of spot-weld points which represent potential high stress areas hence requiring good -quality (low skew) structured meshes connecting them. Most part of the industry accomplishes such meshes through tedious, inefficient, manual techniques.

4. Transfinite Interpolation in 2D Space

Figure 3 depicts a typical 4 sided area that needs to be transfinite meshed. The area is four-sided and require nodes to match up on each pair of “logical” sides.

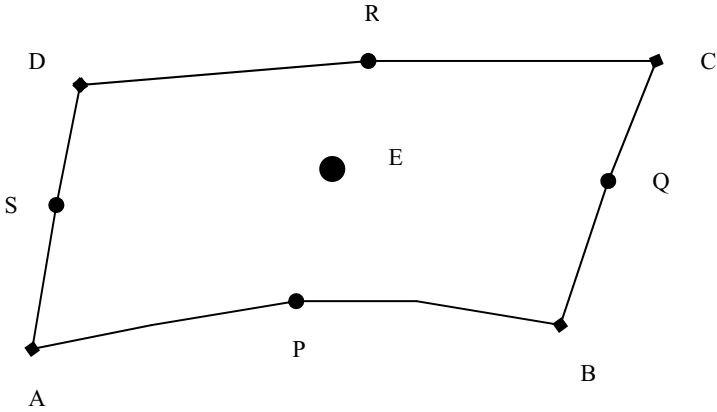


Fig. 3. A 4-sided Coons space

4.1 Coons Blending

Given an area bounded by three or four curves (B-Spline/Bezier) , a surface patch can be created by blending the boundaries using suitable blending functions [11]. The theory of patches and blending was first developed by Coons [12]. Coons blending functions are traditionally used to generate transfinite or mapped meshes on 2D and 3D representation of surfaces or mesh-domains. A 2D four-sided area bounded by four curves (B-spline, Bezier or discrete) as shown in Fig.3. Let P,Q,R,S be functions representing the boundary curves in any cartesian 2D space. Thus,

$$P \equiv Q \equiv R \equiv S \equiv f(x,y) \tag{1}$$

and the rail points are

$$P(x,y) \equiv r(u,0), \quad Q(x,y) \equiv r(u,1), \quad R(x,y) \equiv r(0,v) \text{ and } S(x,y) \equiv r(1,v) \tag{2}$$

where $r(a,b)$ is a generic parametric function that represents each boundary curve in the range of a to b . Also at any point on the boundary curves the cartesian functions can be written as

$$P(x,y) \equiv (P_x, P_y) \tag{3}$$

The corners of the area are denoted by A,B,C,D where

$$A(x,y) \equiv r(0,0), B(x,y) \equiv r(1,0), C(x,y) \equiv r(1,1) \text{ and } D(x,y) \equiv r(0,1) \quad (4)$$

Thus, for any interior node $E(x,y) \equiv r(u,v)$, Coons bilinear blending function can be written as a bullean sum.

$$\begin{aligned} E_x &= (1 - v)P_x + vQ_x + (1 - u)R_x + uS_x - [(1 - u)(1 - v)A_x \\ &\quad + (1 - v)uB_x + v(1 - u)D_x + uvC_x]; \\ E_y &= (1 - v)P_y + vQ_y + (1 - u)R_y + uS_y - [(1 - u)(1 - v)A_y \\ &\quad + (1 - v)uB_y + v(1 - u)D_y + uvC_y]; \end{aligned} \quad (5)$$

In a matrix form, equation (5) can be rewritten for the abscissa as

$$E_x = \begin{bmatrix} -(1-u)(1-v) \\ -u(1-v) \\ -uv \\ -v(1-u) \\ (1-u) \\ u \\ v \\ (1-u) \end{bmatrix} \{\phi\} = [B] \{\phi\} \quad (6)$$

where

$$\{\phi\} = \{ A_x, B_x, C_x, D_x, P_x, S_x, Q_x, R_x \}^T \quad (7)$$

A similar companion equation exists for the ordinate E_y .

4.2 Presence of Interior Point Constraint

If an interior point constraint $F(x,y) \equiv r(u',v')$ exists in the domain closest to node E, (as exhibited in Fig. 1) node E will have to be snapped to location F. The deviation of mesh node E from point constraint F can thus be expressed as

$$f(u,v) = [B] \{\phi\} - F_x \text{ and } g(u,v) = [B] \{\phi\} - F_y \quad (8)$$

As explained before, the aim of this exercise is to minimize the the functionals f,g with respect to u,v as described in eqn. (8). For n interior mesh-points, the problem can be globally described by

$$b = \text{Min}_{(u,v)} \left(\sum_i^n f_i, \sum_i^n g_i \right) \tag{9}$$

The minimization problem can further be expressed as

$$\{f_i \ g_i\}^T = \begin{bmatrix} J_{11} & J_{12} \\ J_{21} & J_{22} \end{bmatrix}^T \{\Delta s_i \ \Delta t_i\}^T \tag{10}$$

Although, this approach has an easy and logical extention in 3D, the 2D approach is mostly used. A 2D domain of the curved surface is developed (or parameter space used) and the mesh is generated in 2D using the improved algorithm. Once the mesh is generated in 2D, a transformation mechanism is used to get the 2D mesh on the 3D surface. This is a standard procedure for generating 2D meshes on developable surfaces and is done no differently for this case.

5. The Inverse Problem and Its Solution

The present scenario leads to an inverse problem as posed by equation (9). During transfinite meshing, Coons equation (6) is used to locate a mesh interior point in the cartesian 2D domain, when its boundary parametric ([B]) and cartesian coordinates ($\{\phi\}$ are known. With the interior point constraint this problem is reversed. The parametric coordinates (u',v') need to be determined while its cartesian location $F(x,y)$ is known.

In order to solve eqn. (10), a modified Newton-Raphson procedure may be adopted.

Using a modified Newton-Raphson, the solution is given by

$$[J] \Delta Z + F = 0 \tag{11}$$

where $[J] = \text{Jacobian} = \begin{bmatrix} J_{11} & J_{12} \\ J_{21} & J_{22} \end{bmatrix}$ (12)

$$\Delta Z = \{ \Delta s, \Delta t \}^T; \quad F = \{f, g\}^T; \tag{13a}$$

The elements of the Jacobian can be expressed as

$$J_{11} = \delta f / \delta s; \quad J_{21} = \delta g / \delta s \tag{13b}$$

$$J_{12} = \delta f / \delta t; \quad J_{22} = \delta g / \delta t \tag{13c}$$

Finally, the change in the parametric coordinates during the i th iteration step can be written as

$$\Delta s_i = (-J_{22} f_{i-1} + J_{12} g_{i-1})/|J| \tag{14a}$$

$$\Delta t_i = (J_{21} f_{i-1} - J_{11} g_{i-1})/|J| \tag{14b}$$

Iteratively solve the following equation, till it converges

$$(s, t)_i = (s, t)_{i-1} + (\Delta s_i, \Delta t_i) \tag{15}$$

6. Solution Convergence

The solution to eqn. (9) is usually quite speedy and usually converges for an error norm $|\epsilon_i| \leq 1e-05$. The error norm $|\epsilon|$ is a root-mean-square of the collective differences of the evaluated coordinates across successive iterations and can be expressed as

$$|\epsilon_i| = (s_i - s_{i-1})^2 + (t_i - t_{i-1})^2 \text{ for the } i\text{th iteration.} \tag{16}$$

However, the convergence of the solution depends on the geometry of the boundary. If the rail curves are represented by higher order rational splines, the solution could slow down a bit; it could slow down a little further if the face is represented by facets (implying the boundary curves are represented by poly-lines). However, for all practical purposes the solution time is insignificant compared to the mesh generation time on these surfaces.

7. Boundary Reflection

Once the inverse problem is solved, the parametric coordinates of the interior points are known in the Coons' domain. These parametric coordinates are now used to create reflected locations on the boundaries of the domain. Figure 4 shows two face interior constraints E and F whose parametric locations in the Coon's space are given by E (s_1, t_1) and F (s_2, t_2) . The solution to the inverse problem gives us the Coon's parametric locations of these points.

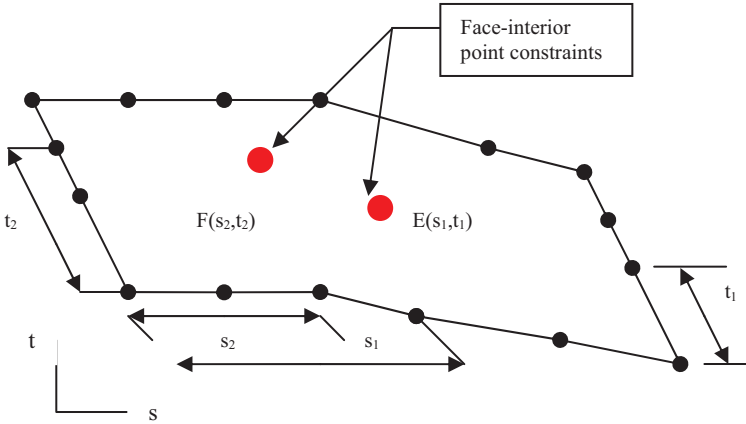


Fig. 4. Interior point constraints reflected on the boundary via “soft-points”

7.1 Soft Points and Pseudo-Edges

The Coons space parametric coordinates of interior points E & F are next used to create 4 temporary nodes on the rail curves at parametric locations s_1, s_2, t_1 and t_2 . These nodes act as “soft-points” or soft-constraints. These soft points need to be honored during boundary discretization. i.e. mesh nodes need to be created at these locations. As a result, it is ensured that the interior points are always reflected on the boundary. The resulting transfinite mesh lines thus flow through the interior point constraints. It is important to note that when 2 or more soft-point locations are close enough on a given pair of sides, they are merged into one.

For every interior point constraint, 4 such soft-points need to be created on the 4-sides of the area. Each side of the 4-sided area is called a “Pseudo-Edge”. It is important to remind here that each pseudo-edge is actually a collection of one or more CAD edges. When the pseudo-edge is discretized, the soft-point acts like a “pseudo-vertex”. A node is always created on it. This ensures, that when a pseudo-edge with a given element count is discretized, these “soft” locations are guaranteed to get a node. The resulting mesh, gets interior nodes that are very close to the face-interior constraints. These nodes are now snapped to the constraint location.

Conventional mesh relaxation methods try to solve the same problem, but they would hold the boundary nodes fixed. The present algorithm, in contrast, determines apriori suitable boundary node locations so as to

minimize the distortion of the mesh. Because there is more freedom on the boundary, with the present algorithm, the chances of producing a better structured mesh is stronger.

7.2 Boundary Discretization

When face-interior point constraints are present, boundary discretization changes in a two-fold manner. Firstly, it creates a non-uniform seeding in most cases, secondly it alters the element count on a given pair of sides. The maximum element count on a side or a Pseudo-Edge can be given by

$$m_i = \lfloor (L_i/s) , (n + 1) \rfloor_{\max} \tag{17}$$

where

m = element count on pseudo-edge i

L_i = length of pseudo-edge i

n = number of unique boundary reflections on a side

s = meshing size

A pseudo-edge is an assembly of p edges. However, when this pseudo-edge is pre-discretized with q soft-points (reflected location of face-interior constraints), the edge is assumed to be logically composed of $r = (p + q)$ sub-edges. The 3D coordinates of node j to be placed at parametric location s_j can be expressed as

$$N_j(x,y,z) = (1 - s_{ij}).P_{ls}(x,y,z) + s_{ij}.P_{le}(x,y,z) \tag{18}$$

where this node is found to lie on the l -th sub-edge; s_{ij} represent its local parametric co-ordinate on the l -th sub-edge; P_{ls} and P_{le} signify the start and end locations of the l -th sub-edge. The local parametric location is given by

$$s_{ij} = \left(s_j \cdot l_{tot} - \sum_{k=1}^{l-1} l_k \right) / l_l \quad \text{where } l_{tot} = \text{length of the } r \text{ sub-edges} \tag{19}$$

l_l = length of the l -th sub-edge that contains this node

7.3 Boundary Blending

We have already observed that presence of interior point constraints affects the boundary discretization of the face. Because interior points are

reflected on the boundary, the boundary discretization becomes non-uniform. When boundary node distribution becomes non-uniform, a boundary blended bi-linear transfinite interpolation becomes necessary to make sure that the mesh line flow is smooth and boundary effects are well reflected in the interior of the space. Coons eqn. (5) now changes to

Thus, for any interior node $E(x,y) \equiv r(u,v)$, Coons bilinear blending function can be written as a bullean sum.

$$E_x = (1 - v')P_x + v'Q_x + (1 - u')R_x + u'S_x - [(1 - u')(1 - v')A_x + (1 - v')uB_x + v'(1 - u')D_x + u'v'C_x]; \quad (20a)$$

$$E_y = (1 - v')P_y + v'Q_y + (1 - u')R_y + u'S_y - [(1 - u')(1 - v')A_y + (1 - v')u'B_y + v'(1 - u')D_y + u'v'C_y]; \quad (20b)$$

where the boundary modified parametric coordinates can be written as

$$u' = \{(1 - \eta)u_1 + \eta u_2\} / \{1 - (u_2 - u_1)(v_2 - v_1)\} \quad (21a)$$

$$v' = \{(1 - \psi)v_1 + \psi v_2\} / \{1 - (u_2 - u_1)(v_2 - v_1)\} \quad (21b)$$

where u_1, u_2 represent the parametric coordinates of the pair of guide nodes on the u -rail curves and v_1, v_2 represent the corresponding parameters on the v -rail curves. ψ and η represent the u and v -directional coordinate for this (u,v) Coons space location assuming a uniform boundary distribution.

8. Examples and Discussion

Figure 5 depicts a flat semi-annular surface with 6 interior point constraints. In automobile body panels, such point constraints usually represent spot-welds. A transfinite mesh of size 5 length units is generated on the surface. The mesh nodes nearest to the point-constraints are snapped to them. As a result, the quad element quality, especially around the spot-welds deplete. The only work-around is to reduce the element size and create a finer mesh so as to reduce element distortion.

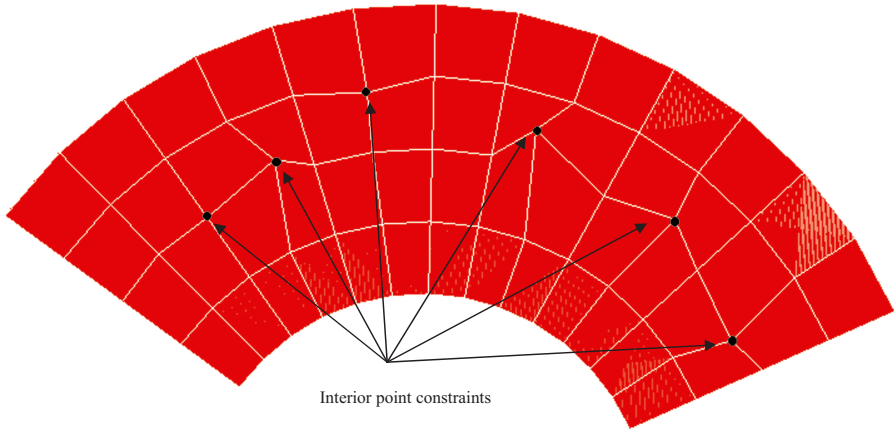


Fig. 5. Unconstrained transfinite (mapped) mesh with interior points. After the mesh is generated, nearest interior nodes are snapped to the point constraints.

Figure.6 shows an improved transfinite mesh that honors the point constraints. Although the element size is same, the interior point constraints are reflected on the boundary. Consequently, the number of elements in the t direction change (from 4 to 6). Since the number of face-interior points is less than the element count in the s direction, the final element count in the s direction does not change (13). It is interesting to note here, that although the elements produced by the algorithm in Fig. 6 are structured compared to the elements around the constraints in Fig. 5, the mesh aspect ratio becomes non-uniform. In most structural analyses, especially of such seam/spot welded body panels, the accuracy of stress computation is most sensitive to element distortion. This, distortion (D) is usually measured as a positive ratio of the minimum to the maximum Jacobian measured at the Gauss points as

$$D = | J_{\min}/J_{\max} | \quad (22)$$

The distortion D , thus, depends little on the aspect ratio of the element, as long as the element shape is rectangular. However, elements too thin (high aspect ratio) tend to have a negative impact on the assembly stiffness matrix. A 5:1 aspect ratio is usually used as a limit. Within this limit, a mesh with a better element distortion (Fig. 6) is deemed more reliable than the unstructured pattern (Fig. 5).

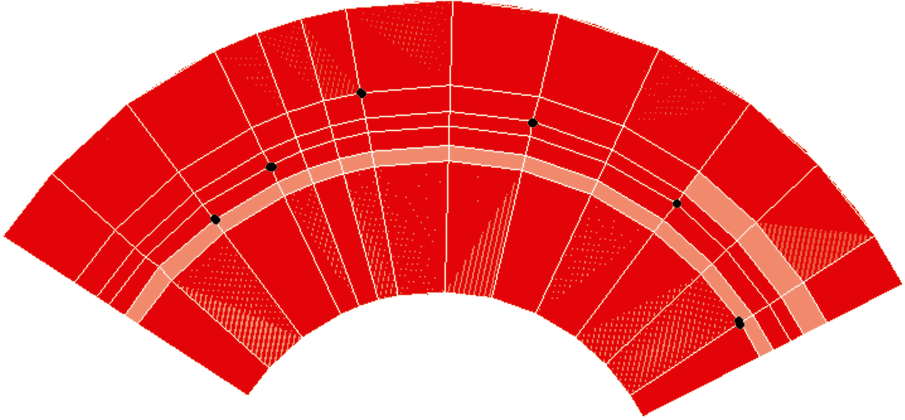


Fig. 6. Improved transfinite (mapped) mesh with interior point constraints.

The following example has 6 interior point constraints, but Fig. 6 shows only 5 soft-points in the radial (t) direction on each pseudo-edge. This is because, two soft-points per pseudo-edge in the t -direction, were merged into an average location because they were too close. As a result, those two point constraints lie on the same nodal rail-line as shown in Fig. 6. This is an example of a practical compromise that needs to be made when one or more constraints are “equi-potential”.

Figure 7 shows a quarter section of a structural bearing which is being analyzed for stress variations under dynamic loads. A swept hexahedral mesh is generated on the volume, where one of the wall faces has 3 interior point constraints. The hex mesh nodes are snapped to the point constraints. 2D transfinite meshes are first generated on all wall faces before the interior is filled. The point constraints, in this case, represent concentrated radial dynamic loads. The mesh nodes of the transfinite mesh on the wall face are snapped to the point constraints, thus resulting in bad quality hexahedral elements in the vicinity of the load application point.

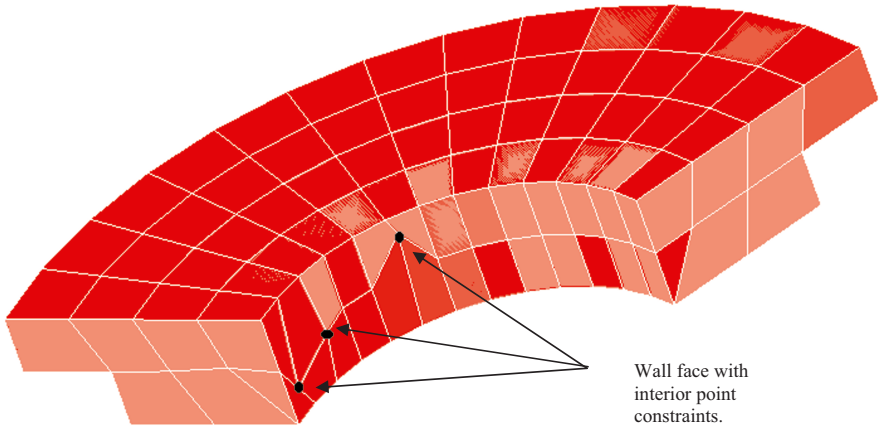


Fig. 7. Swept mesh with face interior point constraints. One wall face shows an unconstrained transfinite (mapped) mesh where the nearest interior nodes are snapped to the point constraints.

Figure 8 shows a much improved hex meshed volume, where the transfinite mesh on the wall face is perfectly structured even though it honors the point-constraints. The resulting mesh has an admirably high mesh quality compared to the mesh in Fig. 7.

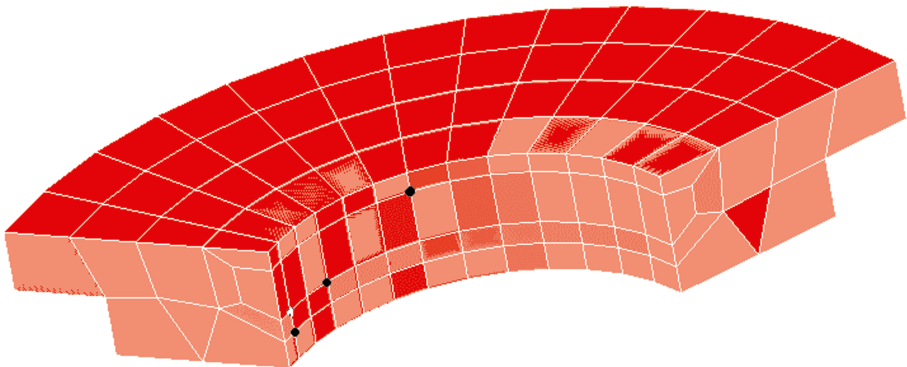


Fig. 8. Improved Swept mesh with face interior point constraints. The transfinite mesh on the wall face is immaculately structured.

9. Conclusion

Structural analyses of automotive parts and body panels frequently require high quality, high fidelity structured meshes. Many of these meshes need to honor pre-defined face-interior and boundary point constraints that represent load application points or welded or joined spots. Conventional meshing techniques snap nearest nodes to these point constraints after meshing is done thus negatively impacting the mesh quality at critical zones of interest. The present paper proposes an apriori remedial approach, where an inverse solution of Coons bi-linear blending equation is performed to determine the parametric co-ordinates of the point constraints. Once the coordinates are known, a boundary correction step is taken, where the boundary of the face is pre-seeded at these parametric locations. The number of elements to be generated along each pair of sides is also influenced by the number and location of point constraints. With the new boundary discretization, a very high quality structured mesh results as is evident from the two examples presented.

References

1. O.C., Zienkiewicz and D. V. Phillips, "An Automatic Mesh Generation Scheme For Plane and Curved Surfaces By Isoparametric Co-ordinates" *International J. Numerical Meth. Engg.* Vol 3 pp. 519-528 (1971).
2. W.J., Gordon and C.A. Hall, "Construction of curvilinear co-ordinate systems and applications to mesh generation" *International J. Numerical Meth. Engg.* Vol 7 pp. 461-477 (1973).
3. W.A., Cook, "Body oriented (natural) co-ordinates for generating three-dimensional meshes" *International J. Numerical Meth. Engg.* Vol 8 pp. 27-43 (1974).
4. Robert, Haber, Mark, S. Shepherd, John, F. Abel, Richard, H. Gallagher and Donald, P. Greenberg "A General Two-Dimensional, Graphical Finite Element Preprocessor Utilizing Discrete Transfinite Mappings" *International J. Numerical Meth. Engg.* Vol 17 pp. 1015-1044 (1981).
5. R. Pierrot, J. Vazeilles and A. Perronnet, "Une methode de generation d'un maillage 2d ou 3d a' partir d'un maillage grossier" *Annales de l'I.T.B.T.P.* Nol 372 (May 1979).
6. A. Perronnet, "Logical and physical representation of an object, modularity for the programming of f.e.m." PDE Software, Interface and Systems, Elsevier Publishers North-Holland IFIP. Soderkoping, Sweden (1984).
7. Alain, Perronnet, "Triangle, tetrahedron, pentahedron transfinite interpolations. Application to the generation of C^0 or G^1 -continuous algebraic meshes" *Proc. Int. Conf. Numerical Grid Generation in Computational Field Simulations. Greenwich, England.* Vol 7 pp. 467-476 (July6-9,1998).
8. Scott, A. Mitchell, "Choosing Corners of Rectangles for Mapped Meshing" *Proc. 13th Annual Symposium on Computational Geometry*, ACM Press, pp. 87-93, (June 1997).
9. Scott, A. Mitchell, "High Fidelity Interval Assignment" *Proceedings, 6th International Meshing Roundtable*, Sandia National Laboratories, pp. 33-44, (October 1997).

10. T.K.H.Tam and Cecil, G. Armstrong, "Finite Element mesh control by integer programming" *International J. Numerical Meth. Engg.* Vol 36, pp. 2581-2605 (1993).
11. G. Farin, *Curves and Surfaces for computer aided geometric design*. Academic Press Inc., San Diego, 1990.
12. I.D. Faux and M.J. Pratt, *Computational geometry for design and manufacture*. Ellis Horwood, Chichester, 1979.

